Data-driven simulations of synoptic circulation and transports in the Tunisia-Sardinia-Sicily region

by

Reiner Onken

SACLANT Undersea Research Centre

Viale San Bartolomeo, 400

La Spezia, Italy

e-mail: onken@saclantc.nato.int

phone: +39-0187-527-349

fax: +39-0187-527-331

Allan R. Robinson, Pierre F.J. Lermusiaux,

Patrick J. Haley, Jr., and Larry A. Anderson*

Harvard University, Cambridge, MA, USA

* now at Woods Hole Oceanographic Institution, Woods Hole, MA, USA

1^{st} revised version

In press, to appear in the *Journal of Geophysical Research*

July 22, 2002

Abstract

Data from a hydrographic survey of the Tunisia-Sardinia-Sicily region are assimilated into a primitive equations ocean model. **The model simulation is then averaged in time over the short duration of the data survey. The corresponding results,** consistent with data and dynamics, are providing new insight into the circulation of Modified Atlantic Water (MAW) and Levantine Intermediate Water (LIW) in this region of the Western Mediterranean. For MAW, **these insights include** a southward jet off the east coast of Sardinia, anticyclonic recirculation cells on the Algerian and Tunisian shelves, and a secondary flow splitting in the Strait of Sicily. For the LIW regime, a detailed view of the circulation in the Strait of Sicily is given, indicating that LIW proceeds from the Strait to the Tyrrhenian Sea. No evidence is found for a direct current path to the Sardinia Channel. **Complex circulation patterns are validated by two-way nesting of critical regions**. Volume transports are computed for the Strait of Sicily, the Sardinia Channel and the passage between Sardinia and Sicily.

1 Introduction

A major task of physical oceanography is to provide a synoptic view of the three-dimensional fields of temperature T, salinity S and velocity for a specific area of the ocean. T and S can be easily obtained by profile measurements with sufficient accuracy and spatial resolution, but the determination of the velocity field is problematic. Currentmeter moorings may provide accurately the vertical structure of the velocity field, but they are expensive and in practice it is not feasible to cover a larger area in order to gain insight into the horizontal variability of the flow field. These shortcomings do not arise with acoustic Doppler current measurements, but these data can be contaminated by high-frequency fluctuations due to surface or internal waves or ship motions. Hence, it is common practice to derive indirectly the geostrophic flow from the observed T and S distributions, however, this method has several deficiencies based on the inherent constraints (stationary, linear, inviscid), some of which may cause incorrect results in special situations. In addition, the theory provides only the vertical shear of the geostrophic flow, and conversion to absolute velocities requires the rather arbitrary assumption of a reference velocity. Special problems do arise in the case of complicated bathymetry. Because the geostrophic vertical shear is proportional to the horizontal density gradient, the horizontal resolution of the T and S profiles has to be sufficiently high in order to resolve strong bathymetry slopes. Otherwise, further dubious assumptions must be made on the density structure below the common vertical range of the profiles.

A first approach to overcome some of the problems is to evaluate the three-dimensional density field from the observed T and S distributions by objective analysis, then derive the geostrophic currents accordingly, and finally mask out the vertical ranges below the

seabed. In the recent past, **this method was frequently used for the initialization of primitive-equation models** [*Robinson*, 1996, 1999; *Robinson et al.*, 1999; *Robinson and Sellschopp*, 2001; *Onken and Sellschopp*, 2001], providing geostrophic currents everywhere, also in regions where no **synoptic** casts were available. *Onken and Sellschopp* [2001, to be referred as OS2001] applied it to a high-resolution quasi-synoptic data set of CTD (Conductivity-Temperature-Depth) and XCTD (expendable CTD) profiles collected in the Tunisia-Sardinia-Sicily region. On the one hand, the results looked promising because the geostrophic flow field matched rather well the distribution of scalars in the core layers of the three dominant water masses MAW (Modified Atlantic Water), WIW (Winter Intermediate Water), and LIW (Levantine Intermediate Water). On the other hand, the velocity pattern was partly not convincing because it contradicts previous knowledge or violated dynamical constraints, mainly in near-shore areas or over complicated bathymetry. For example, it is nowadays generally accepted that the outflow of LIW from the Strait of Sicily to the Tyrrhenian Sea is confined to a narrow channel off the Sicilian west coast (Fig. 1), making an anticyclonic turn around Sicily [*Millot*, 1999; *Astraldi et al.*, 1999; *Sparnocchia et al.*, 1999; *Lermusiaux and Robinson*, 2001]. This feature was not reproduced by the geostrophic calculations. In addition, along the shelf slopes off Algeria and Tunisia, one would expect a boundary current-like LIW flow; instead, the geostrophic velocity pattern exhibited significant on-slope components. Possible reasons for these deficiencies are insufficient data coverage, or the LIW flow is strongly controlled by friction or higly non-linear.

In the present paper, to shed more light on the circulation of water masses in the Tunisia-Sardinia-Sicily region, we are presenting results of a different approach **than that used in OS2001**. The same CTD and XCTD data **are utilized**, but they are assimilated

into an ocean model, providing solutions which satisfy both primitive equation dynamics and observations, also in unsampled regions. In particular, the model results offer consistent solutions of near-slope boundary currents and flow over complicated bathymetry, both of which could not be obtained from geostrophic analysis. In order to achieve synopticity, the model solutions are then time-averaged over the duration of the hydrographic survey, enabling reliable calculations of the transport of volume between the Algerian Basin, the Tyrrhenian Sea and the Eastern Mediterranean.

2 Model description

The Harvard Ocean Prediction System (HOPS) is used for the present study. Although the heart of HOPS is a primitive equations model, it is called a "system" because it contains various program packages which are necessary for setting up the model domain and the grid, conditioning of bathymetry, management of observational data, objective analysis, preparation of assimilation fields, etc. [*Robinson*, 1996, 1999; *Robinson et al.*, 1996; *Lozano et al.*, 1996]. In the following, the modules of HOPS described are only those used for the model simulations presented below.

2.1 The primitive equations model

The dynamical model used in this study solves the primitive equations (PE), assuming that the fluid is hydrostatic and the Boussinesq approximation is valid [*Spall and Robinson*, 1990; *Lermusiaux*, 1997]. In the horizontal, it applies open boundary conditions for tracers and velocity based on *Orlanski* [1976], and for vorticity and transport according to *Spall and Robinson* [1990]. The vertical boundary conditions are that of no normal

flow at the surface (rigid-lid) and at the bottom.

Horizontal subgridscale processes are parameterized by a 2-1-1 (second order, one times, every time step) Shapiro filter [*Shapiro*, 1970; *Robinson and Walstad*, 1987] for momentum and tracers. Vertical diffusion is formulated in terms of a Richardson-number dependent scheme similar to that of *Pacanowski and Philander* [1981], using a maximum value of $50\,\mathrm{cm^2 s^{-1}}$ for eddy viscosity when the Richardson number is zero or when the water column is gravitationally unstable. Near horizontal and vertical rigid boundaries, Rayleigh friction is applied using a Gaussian weighting of distance from the bottom or the coast, respectively [*Lermusiaux*, 1997].

2.2 Domains, bathymetry and grid setup

From preliminary model runs it had turned out that complex current patterns evolved around Sardinia and in the Strait of Sicily. In order to validate that these patterns are real and not due to insufficient horizontal resolution or truncation errors in the pressure gradient calculation over steep topography (see below), we defined a large and two small model domains, referred to as "Sardinia (sub)domain" and the "Sicily (sub)domain". The latter were two-way nested into the large domain and are providing a zoom into regions of special interest (see Fig. 1 for the positions of the subdomains).

The large model domain is almost identical with the boundaries of the survey area as defined by OS2001. In zonal direction, it extends from 7°E to 12.5°E, and the meridional boundaries are 36.5°N and 39.5°N, respectively. The bottom is defined by the DBDBV bathymetry data set (obtainable from the Naval Oceanographic Office, Stennis Space Center, Mississippi, Internet address "http://www.navo.navy.mil/") providing $1'$ horizon-

tal resolution. At 38°N, this is equivalent to 1852 m in meridional and 1459 m in zonal direction. In order to make optimal use of this data, a horizontal grid size of 1500 m was selected, yielding 325 grid points in west–east and 225 points in south–north direction.

Vertically, the large domain is divided in 35 levels defined in terms of terrain-following single σ-coordinates [*Spall and Robinson*, 1989; *Haley*, 2001]. The use of such coordinates requires careful handling of the bathymetry data. First of all, the data are interpolated on the model grid and all elevations above -10 m are clipped. This is because the minimum depth to be resolved by the model was set to this value, in part to prevent crowding of σ-levels. Then, land points are re-introduced by superposition of a high-quality coastline data set. Small-scale roughness is removed by repeated median filtering, before the vertical levels are defined. Here, special care must be taken that the hydrostatic consistency condition is guaranteed in order to reduce the truncation error of the pressure gradient calculation to tolerable levels [*Haney*, 1991; *Lozano et al.*, 1994; *Sloan*, 1996]. As this condition is proportional to σ, the gradient of the bathymetry and the horizontal grid size, it can either be satisfied by optimized positioning of the σ-levels or by reduction of the bathymetry slope or both. In the present case, our objective was to keep high vertical resolution in the upper 700 m depth range. Therefore we did not optimize the σ-levels but reduced the bottom slope instead to a maximum value of 6% using a Gaussian filter. This preserved most of the bathymetric details (Fig. 1). The final arrangement of σ-levels is such that in the worst case at the position of the deepest depth (3444 m, in the Tyrrhenian Sea), the vertical resolution Δz increases from about 14 m near the sea surface to 550 m at $z = 2500$-m depth, and then decreases again towards the bottom (Fig. 2). Everywhere else the resolution is better. This is sufficient to resolve the vertical layering of water masses.

The Sardinia domain (Fig. 1) extends from 8.07°E to 9.92°E east–west and from 38.56°N to 29.44°N in south–north direction; the corresponding limits for the Sicily domain are 10.87°E – 12.12°E and 37.21°N – 38.21°N, respectively. The horizontal resolution of the subdomains, i.e. 500 m, is three times that of the large domain and the horizontal grid points are arranged in a way that every third is colocated with a grid point in the large domain. The vertical coordinates are the same in all domains, and identical parameters were used for filtering the bathymetry and reduction of bottom slope. In addition, in order to guarantee a smooth transition between the subdomains and the large domain, the land masks and the bathymetry were aligned near the boundaries.

2.3 Initialization

The initial mass field of the models is generated by mapping observed T and S data on the horizontal grids, and the initial velocity fields ar defined in terms of the corresponding geostrophic currents. The data, consisting of CTD and XCTD casts collected in the period 19 – 29 October 1996, are identical to those used by OS2001 for their geostrophic analysis. The position of the casts is shown in Fig. 3.

Using objective analysis (OA) [*Carter and Robinson*, 1987; *Lozano et al.*, 1996; *Lermusiaux*, 1999a], T and S are mapped on the model horizontal grids at 65 horizontal levels, spaced 10 m apart between the sea surface and 500-m depth, 20 m between 500 m and 600 m, and 50 m between 600 m and 1000 m. No further levels are defined below 1000 m, because only six casts extended beyond that depth. The OA applies a time-independent, isotropic Gaussian correlation function (cf. *Robinson and Golnaraghi* [1993]), using an e-folding scale of 40 km, which is a compromise between the internal Rossby radius as a

"natural" correlation scale and the resolution of the observational data. The mean field which has to be removed prior to the OA, was estimated by OA using an e-folding scale of 100 km.

The objectively analyzed fields are interpolated vertically on the σ-levels, leaving them constant below 1000-m depth. Geostrophic currents are calculated relative to a reference level, and a barotropic transport streamfunction is estimated from this flow field. Previous experiments [*Robinson and Golnaraghi*, 1993] have shown that the model behaves best when the conversion from barotropic to baroclinic energy is minimized during the first days of the integrations. This is the case when selecting 550 m as level of no motion. For physical reasons, the streamfunction of the large domain was evaluated in two steps. A first calculation was based solely on the interior geostrophic velocity field, which generally produces non-zero net transport across each open model boundary. In the present case, there was a net inflow of 0.45 Sv (1 Sv=10^6 m^3s^{-1}) from the Eastern to the Western Mediterranean. Because the long-term net exchange between both basins should be approximately zero (the evaporative water loss over the Eastern Mediterranean is equivalent to about 0.06 Sv, cf. *Bethoux* [1980]), the excess transport was removed by subtracting a linear streamfunction along the southeast boundary between Sicily and Tunisia. To close the budget, the same 0.45 Sv were added linearly to the net inflow along the northwest boundary between Algeria and Sardinia, making it in total 0.39 Sv to the east. This amount leaves the domain across the northeastern open boundary, representing the net loss from the Tyrrhenian to the Ligurian Sea via the Corsica Channel. According to *Astraldi et al.* [1994], the number is fairly close to what has been observed during this time of the year. In the second step, the streamfunction was evaluated once more, but now taking account of the constraints imposed along the open boundaries. **For the subdomains,**

the initial streamfunction was estimated in the same way but constrained to the conditions imposed by the large domain along their open boundaries.

Before starting the actual model simulations, a zeroth-order estimate of the systematic truncation error or pressure gradient bias occurring in the interpolation of the pressure gradient from the horizontal (flat) to the sigma coordinates is computed as follows [*C.J. Lozano*, personal communication; *Lermusiaux*, 1997). The initial T and S fields are first horizontally averaged and the corresponding pressure gradient on sigma coordinates is then computed by integrating the model over one time-step. During a dynamical model evolution, this pressure gradient, which is not exactly zero due to truncation errors, is the zeroth-order estimate of the total bias which is added to the solution at every time-step. Therefore, in the present model simulations, this estimate is subtracted at every time-step. Finally, the model clock is set to 18 October 1996 00:00h (UTC) and the PE integration begins using a time step of 216 s (400 steps per day) for all domains. The integration is continued for 12 days until 30 October 00:00h.

2.4 Data assimilation and atmospheric forcing

At initialization time, the flow field of the models is balanced by the pressure field alone, but it is not in balance with inertial and frictional forces. The full dynamical balance is achieved after an adjustment phase of the order of a few days (cf. *Robinson* [1996], *Lermusiaux and Robinson* [2001]). During this phase, the flow field is subject to inertial oscillations and "forgets" the level of no motion. One is tempted to analyze the model flow field when the adjustment is finished, but at that time the initial mass field may have changed already. In order to prevent this, the observed T and S are repeatedly

assimilated into the model during integration.

Optimum interpolation [*Robinson et al.*, 1998] is the assimilation method used here. For that purpose, objectively analyzed fields of T and S are prepared for the entire survey period in 24h-intervals and centered in time at the beginning (midnight) of every day. In total, 11 fields are available 19–29 October. The same 65 horizontal levels and spatial correlation scales as above are applied, but in addition the data are weighted in time using a temporal correlation scale of 10 days. Hence at every OA time level, the strongest weighting is assigned to those data nearest in time. After vertical interpolation on the σ-levels, each of these cycles is assimilated into the model ten times in 2.4-hours (= 1/10 day) intervals, with linearly increasing weight when approaching the nominal time of the OA. For example, cycle 1 is assimilated for the first time on 18 October 02:24h using a weighting coefficient of 0.1; the second assimilation of the same cycle is at 04:48h but now using a weight of 0.2. The tenth and final assimilation of cycle 1 takes place at its nominal OA time on 19 October 00:00h, applying the full weight of 1. Beginning at 02:24h of the same day, the same procedure is repeated for cycle 2, again starting with weight 0.1, etc. By this method, the model solution is relaxing towards the data in space and time.

At the sea surface, the models are driven by 6-hourly windstress provided by the European Centre for Medium Range Weather Forecast (ECMWF, Reading, United Kingdom). As can be seen from Fig. 4, the stress was rather low never exceeding 0.1 N m^{-2} after October 22. Heat and freshwater fluxes were not available, but that does not seem to be critical; as the survey took place in October, it is conjectured that the net heat flux is approximately balanced, and, for the short integration time, the surface fresh water flux is expected not to be important.

2.5 Nesting

Two-way nesting means that a large domain and a nested subdomain are running synchronously on a computer, exchanging information at each time step. When the calculations of one time step are finished, the large domain provides the prognostic variables for the subdomain along the common boundaries, then the subdomain runs one time step and returns information to the large domain. The latter feedback is accomplished by averaging of the prognostic volume data of the subdomain "horizontally" on σ-levels on the large domain horizontal grid. In this way, the large domain is driving the subdomain through the boundaries, while the large domain "learns" something about the small scale physics in the subdomain, which cannot be resolved by the coarse grid. Another important consequence of the feedback is that no independent solution can evolve in the subdomain.

HOPS is designed to run multiple nested domains at a time, but only if they are arranged in a telescoping way. In our case, the Sardinia and Sicily subdomains are both nested into the large domain at the same nesting level, hence they cannot be integrated simultaneously. Therefore, in order to provide a unique solution for the large domain, we will discuss in the following only the results of the "standalone" large domain without any nesting. The results of the subdomains will be recalled only for validating the results of the large domain in critical areas.

3 Horizontal flow

In this section, we are presenting horizontal flow patterns of MAW and LIW, and compare them with the results obtained by OS2001. Based on six-hourly model outputs, currents have been time-averaged over the integration period of the model **between 19 October 18:00 and 30 October 00:00. Hence, the spin-up phase (36 hours ≈ 2 inertial periods) was skipped, because the full dynamical balance may not yet have been achieved.** Differently to OS2001, the flow fields were here not averaged vertically over the corresponding water mass range in order to provide more insight into details. Instead, MAW currents were determined **at a shallow constant depth level** and those for LIW at the salinity maximum.

3.1 MAW

Fig. 5 shows the flow field at 30-m depth. This level lies well within the MAW (cf. OS2001) and is supposed not to be directly affected by the windstress. Both qualitatively and quantitatively, the PE and geostrophic (cf. Fig. 4 of OS2001) current patterns exhibit many similarities; this is the jet-like eastward flowing Algerian Current along the Algerian/Tunisian shelf break, the flow splitting at about 10.5°E, the strong southward current off Cape Bon, the cyclonic recirculation in the Tyrrhenian Sea, and the vortices west of Sardinia, in the Sardinia Channel, between Sicily and Cape Bon and northwest of Sicily. Further agreement concerns the impact of topographic obstacles on the Algerian Current; the current is circumventing Galite Plateau, but obviously the flow path is not significantly altered by Skerki Bank. However, from the PE model there is evidence that Skerki Bank may support the flow splitting at 10.5°E.

The most noticeable difference between the PE results and OS2001 is the narrow ≈ 10 km wide jet off the southeast coast of Sardinia. The jet is most intense at the surface reaching a core speed of almost 35 cm s^{-1} , while at 100-m depth the speed is less than 5 cm s^{-1} . From the geostrophic analysis, there is no indication for such feature, apparently because of lack of hydrographic casts close to the coast. It is also not supported by the few acoustic Doppler measurements (cf. Fig. 5 of OS2001). **Probably, as the nearest approach of the Doppler measurements to the eastern Sardinian coast was about 6 km, the jet was not caught, the width of which is ≈ 6 km in Fig. 5 at this location (for more see below and Fig. 6).** The only indication of the existence of such "East Sardinia Current" is gained from earlier observations [*Krivosheya and Ovchinnikov*, 1973; *Krivosheya*, 1983]. The PE results are also providing additional information on the Algerian Current and the structure of flow over the Algerian/Tunisian shelf. Comparison of Figs. 5 and 1 reveals that the core of the current follows approximately the 200-m isobath. Anticyclonic recirculation cells over the shelf are supporting strong (up to 30 cm s^{-1}) near-coast countercurrents between 7°E and 9°E, and in the bay at about 10.5°E. Further details of the MAW flow at the entrance of the Strait of Sicily become evident. Here, a secondary splitting occurs at 11.5°E, 37.5°N, elements of which were already identified by *Robinson et al.* [1999] based on data of August of the same year. It is also represented by the model of *Pierini and Rubino* [2001], hence one might conjecture that it is a permanent feature of the local circulation. After that splitting, the larger part of the flow recirculates to southwest and joins the major southward branch between Tunisia and Pantelleria, but a small fraction remains confined to the Sicily coast and apparently feeds the MAW vein off the Sicily south coast frequently mentioned in other publications [*Astraldi et al.*, 1996; *Lermusiaux*, 1999b; *Lermusiaux and Robinson*,

2001].

The most questionable MAW flow pattern is the East Sardinia Current. In order to validate that this feature is neither due to unsufficient horizontal resolution nor to errors in the pressure gradient calculation, Fig. 6 is presenting the mean horizontal flow at 30-m depth from the nested Sardinia subdomain. Comparison with Fig. 5 reveals that all details of the boundary current are matching, i.e. the magnitude of velocity, the width, and its decreasing strength when surrounding Sardinia in accord with the topography. Hence, this feature is not an artifact of the large domain model setup.

3.2 LIW

At every point of the horizontal model grid, LIW currents were interpolated vertically from the model σ-levels onto the depth of the salinity maximum S_{max} as determined by OS2001 (see their Fig. 9 and the inset map of Fig. 7). Comparison of the results shown in Fig. 7 with the vertically averaged geostrophic LIW flow in OS2001 (their Fig. 10) exhibits many similarities, predominantly in the deep basins. Here, the PE model clearly reproduces the cyclonic recirculation in the southern Tyrrhenian Sea, **the anticyclone southeast of Sardinia**, the anticyclonic flow around that island, and the eddy dipole between 37°N and 38°N close to the western boundary of the model domain. Also the strength of the currents is roughly the same — a few centimetres per second. **Slightly different are the currents in the Sardinia Channel. Here, the PE currents are heading to southwest, whereas the geostrophic calculation yields a more southward direction. The difference is perhaps due to the selection of the level of no motion or the vertical averaging in OS2001.**

Major differences show up along the African shelf, between Skerki Bank and Galite Platau and in the Strait of Sicily. This is not surprising, because non-linearity and friction certainly play a significant role in these regions. All along the shelfbreak between 8.5°E and 9°E, there is a LIW boundary current in the PE model, heading from the Sardinia Channel to the Algerian Basin. It is about 10 km wide and the maximum speed is close to 10 cm s^{-1} . No such flow is reproduced by the geostrophic calculations. Between Galite Plateau and Skerki Bank, the geostrophic analysis yielded flow to southwest and unrealistic onshore velocity components. These features are missing from the PE flow field. Instead, the velocities are rather weak and **there is some evidence for a LIW return flow to the Strait of Sicily along the northwestern flank of Skerki Bank.** Currents are most intense in the Strait of Sicily, but the mean direction of geostrophic flow is to the southwest, whereas the PE currents are following the bathymetry in agreement with *Sparnocchia et al.* [1999] **and with** *Lermusiaux and Robinson* **[2001] even though amplitudes are here larger due to the higher model resolution**. In the central part of the Strait, their direction is almost to the north, and towards the Tyrrhenian they attain a more northeastward direction.

More insight into the internal structure of LIW in the Strait is provided by Fig. 8 showing the pattern of salinity and horizontal velocity at increasing depth levels. At 100 m, the salinity lies within the range 37.2–38.1. According to OS2001 (their Figs. 3 and 9), the MAW core salinity is 37.2–37.7 in this area, while that of LIW is almost uniform at about 38.7. Hence, in the southwest corner, the 100-m level lies well within the MAW, while towards northeast there are already significant LIW admixtures. Nevertheless, the pattern of currents exhibits largely MAW characteristics: the MAW flow splitting is clearly visible by means of the northeastward directed low salinity lobe. However, near

Adventure Bank and east of the Marettimo Plateau (see Fig. 8b for geographic names), there is an intense northward boundary current with maximum speeds of up to 50 cm s^{-1} . In Fig. 5, only south of $\approx$ 37.8°N there is evidence for such northerly flow, which was identified as a secondary MAW splitting. In terms of salinity, the next deeper level at 150 m is still within the MAW/LIW transitional regime, but the flow patterns is significantly different from that above. South of 37°20′ N, high salinity water invades the region by means of a broad northward flow about 40 km wide. Maximum velocities here are around 20 cm s^{-1} . A little farther north when approaching topographic obstacles, the flow separates in three branches. The western one turns left around the western rise heading towards Skerki Bank, the eastern branch goes straight north into the deep narrow passage between the central rise and Adventure Bank, and the central is surrounding the central rise anticyclonically and joins the eastern branch downstream. The combined current is then heading along the eastern boundary into the Tyrrhenian, exhibiting maximum speeds of $\approx$45 cm s^{-1} in the passage and still $\approx$20 cm s^{-1} off the Marettimo Plateau.

At 250 m, minimum salinities are close to 38.5 around Skerki Bank, hence the water mass at this depth may be considered as pure LIW. The inflow pattern near the southern boundary is similar to that at 150 m. Constrained by bathymetry, there are again three branches of the current, but it appears that for all of them there is an enhanced tendency to go east as soon as the obstacles have been passed (note the different scaling of the graph). In addition to the concentrated eastern boundary flow, a large part of the flow to the Tyrrhenian is accomplished by a wide current band at about 11°25′ E, which joins the boundary current off the Marettimo Plateau. Because of the limitations due to bathymetry, the latter is the only remaining current at the 400-m level, which (in the model) is already below the sill depth of the southern passages. Concerning salinity, the

horizontal and vertical variations below 250 m are rather small, < 0.4 horizontally and < 0.2 vertically. From the maps, one might guess that the most saline water is sinking to greater depths north of the narrow passages and then fills the deeper portions between Skerki and Adventure Bank.

From Fig. 8, there is no evidence that any flow below 100-m depth goes west across Skerki Bank. This is an important finding concerning the historical discussion whether there exists a short route for LIW from the Strait of Sicily to the Sardinia Channel. This is consistent with the flow at the S_{max} level (Fig. 7) described above, which did not show any organized westward flow west of Skerki Bank. To shed some more light on this matter, Fig. 9 displays in a three-dimensional view the mean flow field around the northeastern extension of Skerki Bank in the LIW vertical range between 150 and 800 m. In the upper left corner, part of the previously mentioned LIW flow to the Tyrrhenian is visible. The strong flow in the upper right is the lower portion of the Algerian Current (cf. Fig. 8a). The jet-like eastward flow attached to Skerki Bank is LIW recirculating from the southern Tyrrhenian Sea (cf. Fig. 7). Apparently, there is no significant westward LIW flow across Skerki Bank, instead there is evidence that part of the recirculating LIW returns to the Strait of Sicily. This is in agreement with OS2001, who found "old" LIW in the Strait.

For validating the complex structures of LIW, Fig. 10 shows the horizontal flow field at 250-m depth obtained from the nested Sicily subdomain (Fig. 1). The flow pattern is almost identical to that of Fig. 8c, hence we are confident that the results of the large domain are correct. Noteworthy is the weak anticyclonic flow around Skerki Bank, providing more evidence for a return flow of low-salinity LIW from the Sardinia Channel to the Strait of Sicily. This pattern did not show up that clearly in the lower resolution standalone

large domain.

4 Volume transports

In OS2001, all attempts failed to evaluate consistent volume transports in the Sardinia Channel, in the Strait of Sicily, and between Sardinia and Sicily. In the light of the model results presented here, this is not surprising because the MAW transport over the Tunisian shelf, the LIW boundary currents, and the impact of topographic steering on the currents are certainly not represented by geostrophic calculations. Therefore, another attempt is made to calculate these quantities from the PE model results.

Volume transports were calculated from the time-averaged PE velocity field for Sections A, B, and C (Fig. 11) representing the boundaries between the Skerki region (i.e. the area within the triangle) and the Algerian Basin, the Estern Mediterranean, and the Tyrrhenian Sea, respectively. The most delicate problem was the definition of water mass boundaries. As water below 1000-m depth was not existent in terms of an own T/S characteristics, the lower LIW boundary was positioned at 1000 m. For the same reasons, we also did not distinguish between different deep water masses known to play a role in this area; the water below 1000 m is just referred to as Deep Water (DW). Hence, the problem was condensed to the definition of a meaningful MAW/LIW interface. It is postulated that such an interface exists, and can be represented by a surface of constant potential density σ_0. In principle, also isohalines could serve for the same purpose as they are almost everywhere aligned with σ_0-surfaces, but σ_0 surfaces are dynamically more meaningful. For each section, transports were calculated for all σ_0 surfaces in the density range $27.4 \leq \sigma_0 \leq 29.05$ in 0.05 kg m^{-3} intervals. Then for Sections A and B,

the isopycnal yielding a transport maximum for MAW and LIW is considered to be the most appropriate interface. The physical reasoning for this method is the assumption that the flow direction of MAW and LIW are opposed to each other. The method fails for Section C because the assumption of MAW/LIW counterflow is not necessarily satisfied. Morever, from previous knowledge one might expect a net inflow into the Tyrrhenian both for MAW and LIW. Therefore, the density of the MAW/LIW interface for Section C was defined to be the mean of the σ_0 values for Sections A and B.

In Section A, maximum eastward MAW transport of 1.8 Sv was found for $\sigma_0 = 28.63$ kg m^{-3} , opposed by westward LIW transport of 1.3 Sv (all transport numbers were rounded to 10^{-1} Sv). Together with a westward DW transport of 0.1 Sv between 1000 m and the bottom (not shown in Fig. 11, cf. Fig. 12), the barotropic transport is 0.4 Sv to the east as required by the streamfunction definition (see above). Both the MAW and LIW transport are higher than those obtained from the few previous investigations which took place in the Sardinia Channel. Based on geostrophic calculations from data sets of different years, *Garzoli and Maillard* [1979] found between 0.22 Sv westward and 0.72 Sv eastward transport for MAW, indicating a large interannual variability. By contrast, their LIW transports around 0.9 Sv (westward) exhibited only little variability. Using the same method, *Sammari et al.* [1999] obtained between 0.6 Sv and 1.3 Sv eastward MAW transport. From salinity budget calculations, *Bethoux* [1980] arrived at 1.85 Sv eastward for MAW and 0.8 Sv westward transport for LIW. A direct comparison of these numbers with our results is questionable, because of the different methods involved. *Garzoli and Maillard* [1979] defined the MAW/LIW interface by the 38.5 isohaline, and *Sammari et al.* [1999] 38.2, both of which appear to be deeper than the 28.62 isopycnal applied here, which corresponds closely to salinity 38.1. According OS2001 (their Figs. 3

and 9), the mean MAW core salinity along Section A is about 37.6 while that of LIW is close to 38.7; therefore it is assumed that 38.1 is an appropriate choice for the MAW/LIW interface.

Because of the constraint of zero net transport through the Strait of Sicily and no DW contribution, MAW and LIW transports in Section B are exactly balanced. Therefore, maximum transport of 1.3 Sv in either direction was found both for MAW and LIW using σ_0=28.20 kg m^{-3} as interface. This value is lower then the σ_0-level in Section A, but for the following reasons it is assumed that the choice of this level is adequate. Fig. 11 shows that the selected isopycnal separates the southward flowing MAW from the LIW regime below heading in the opposite direction. Comparison with Fig. 5 reveals that the northwestward MAW flow in the center of the section are due to the recirculation within the anticyclonic vortex over Adventure Bank. The vertical position of σ_0=28.20 kg m^{-3} is again almost identical to that of the 38.1 isohaline, representing the mean of the MAW and LIW core salinities. The transport numbers presented here are within the limits set by previous investigations. Both for MAW and LIW, these are approximately 0.4 and 3.5 Sv, based on different methods and summarized by *Astraldi et al.* [1996].

Whatever isopycnal was selected, the net transport of both MAW and LIW was always directed from the Skerki region to the Tyrrhenian for Section C. This is in agreement with the few available earlier publications (cf. *Garzoli and Maillard* [1979]; *Astraldi and Gasparini* [1994]). For the MAW/LIW interface selected here at σ_0=28.42 kg m^{-3} , the MAW transport is 0.3 Sv and 0.2 Sv for LIW. Again, the interface level corresponds to salinity 38.1.

The evaluated volume transports are summarized in Fig. 12 (note that the boxes are representing net transports orthogonal to the respective sections; they must not be

identified with pathways of water masses!). Surprisingly — although the transport calculation was not constrained by mass conservation — the budget of each individual water mass within the Skerki region is almost balanced: for MAW, there is a surplus of $1.8 - 1.3 - 0.3 = 0.2$ Sv, while the LIW deficit is $1.3 - 1.3 - 0.2 = -0.2$ Sv. We leave it open for speculation, whether these 0.2 Sv are converted from MAW to LIW or are just due to inadequate selection of the MAW/LIW interface. If the latter is true, they may be considered as an error estimate of the transport calculation for Sections A and B, but not for C! Here, both the net transports of MAW and LIW are always directed towards the Tyrrhenian whatever interface was selected, hence at least for LIW the error is definitely less than 0.2 Sv. The direction of the transports across Section C also makes sense, because it is know from observations (cf. *Astraldi and Gasparini* [1994]) that the Tyrrhenian exports both MAW and LIW to the Ligurian Sea through the Corsica Channel. Moreover, it should be mentioned that for each section the integral transport equals the barotropic transport imposed on the open boundaries of the model, i.e. 0.4 Sv for Sections A and C, and zero for B.

Although it was rather calm during most of time of the 12-days integration period, we calculated the volume transports once more, but from a model run without any atmospheric forcing. The effect is not significant – all transport numbers changed by less than 0.1 Sv. In particular, in Section B the transports of MAW and LIW decreased slightly, while in Section C the MAW transport increased and that of LIW decreased; almost no change occurred in Section A. Recalling Fig. 4, both the reduced MAW transport in Section C and the higher transport in Section B in the wind-driven case may be explained in terms of a southward directed Ekman transport due to the westerly wind

between October 18 and 22.

5 Summary and conclusions

In the present paper, it has been demonstrated that bringing together data and primitive equation dynamics provides a useful tool for the interpretation of oceanographic data. The data originated from an oceanographic survey which took place in the Tunisia-Sardinia-Sicily area in October 1996. Using Optimum Interpolation, they were assimilated into a primitive equations ocean model, taking account of correlation scales in space and time. Employing high horizontal and vertical resolution and the best available information on bathymetry, the ocean model was run over the entire duration of the survey (12 days). All model results were then averaged in time over the duration of the survey and so as to provide a dynamically consistent synoptic view of the circulation of water masses.

The regional circulation features and water pathways computed by this approach are more accurate than what is classically estimated. In particular, they could not have been obtained from the observed data sets alone because of missing observations in denied areas (12-miles-zone), unsufficient resolution in topographically complex regions, and inadequate representation of currents by geostrophic analysis.

For Modified Alantic Water (MAW), anticyclonic recirculation cells over the Algerian/Tunisian shelf were revealed, and there is clear evidence for a return flow from the Tyrrhenian Sea by means of a narrow jet off the Sardinian east coast. Besides the well known splitting of MAW into the Strait of Sicily and the Tyrrhenian Sea branches, the model reproduces a secondary splitting in the Sicily Channel, the northern arm of which

feeds an eastward vein of MAW along the south coast of Sicily. It appears that this secondary split is triggered by topography and the Levantine Intermediate Water (LIW) below.

New results were obtained for the LIW circulation. A detailed description of LIW flow in the Sicily Channel is provided, exhibiting a jet-like boundary current to the Tyrrhenian in the upper LIW and a broad flow below. No indication was found for a direct LIW path from the Strait of Sicily to the Sardina Channel across Skerki Bank.

Complex current patterns around Sardinia and in the Strait of Sicily have been validated by additional two-way nested model runs, employing three times higher resolution in the respective regions.

Volume transports, constrained by known net transports in the Strait of Sicily and the Corsica Channel, have been evaluated for the Strait of Sicily, the Sardinia Channel and the passage between Sardinia and Sicily. While the transport numbers in the Sardinia Channel appear to be higher than those from few available earlier studies, those in the Strait of Sicily are within the limits of previous investigations. For the passage between Sardinia and Sicily, MAW and LIW transports are in agreement with an export of these water masses from the Tyrrhenian to the Ligurian Sea.

Acknowledgments

This work was performed at the SACLANT Undersea Research Centre in La Spezia, Italy. The authors would like to thank the crew of *NRV Alliance*, the technical staff of SACLANTCEN, and the Scientist-in-Charge, Jürgen Sellschopp, for the acquisition of the high-quality in-situ data set. Historical windstress data were kindly provided by the European Centre for Medium Range Weather Forecast in Reading (United Kingdom). This study was supported by the Office of Naval Research under grants N00014-95-1-03371 and N00014-97-1-0239 to Harvard University.

References

Astraldi, M., S. Balopoulos, J. Candela, J. Font, M. Gačič, G.P. Gasparini, B. Manca, A. Theocharis, and J. Tintoré, The role of straits and channels in understanding the characteristics of Mediterranean circulation, *Progr. Oceanogr., 44*, 65–108, 1999.

Astraldi, M., and G.P. Gasparini, The seasonal characteristics of the circulation in the Tyrrhenian Sea, in *The Seasonal and Interannual Variability of the Western Mediterranean Sea, Coastal and Estuarine Studies*, *46*, edited by P.E. La Violette, pp. 115–134, American Geophysical Union, 1994.

Astraldi, M., G.P. Gasparini, and S. Sparnocchia, The seasonal and interannual variability in the Ligurian-Provençal Basin, in *Seasonal and Interannual Variability of the Western Mediterranean Sea, Coastal and Estuarine Studies, 46*, edited by P.E. La Violette, pp. 93–113, American Geophysical Union, 1994

Astraldi, M., G.P. Gasparini, S. Sparnocchia, M. Moretti, and E. Sansone, The characteristics of the water masses and the water transport in the Sicily Strait at long time scales, *Bull. Inst. Océanogr. Monaco*, n°spécial *17*, 95–117, 1996.

Bethoux, J.-P., Mean water fluxes across sections in the Mediterranean Sea, evaluated on the basis of water and salt budgets and of observed salinities, *Oceanol. Acta, 3*, 79–88, 1980.

Carter, E.F., and A.R. Robinson, Analysis models for the estimation of oceanic fields, *J. Atmosph. Ocean. Technol., 4*, 49–74, 1987.

Garzoli, S., and C. Maillard, Winter circulation in the Sicily and Sardinia Strait region, *Deep-Sea Res., 26A*, 933–954, 1979.

Haley, P.J., Jr., GRIDS User's Guide, Harvard University, Cambridge, MA, 45pp, 2001.

Haney, R.L. On the pressure gradient force over steep topography in sigma coordinate ocean models, *J. Phys. Oceanogr., 21*, 610–619, 1991.

Krivosheya, V.G., Water circulation and structure in the Tyrrhenian Sea, *Oceanology, 23*, 166–171, 1983.

Krivosheya, V.G., and I.M. Ovchinnikov, Peculiarities in the geostrophic circulation of the waters of the Tyrrhenian Sea, *Oceanology, 13*, 822-827, 1973.

Lermusiaux, P.F.J., Error subspace data assimilation methods for ocean field estimation: theory, validation and applications, *Harvard Open Ocean Model Reports, 55*, Harvard University, Cambridge, MA, 402pp, 1997.

Lermusiaux, P.F.J., Data assimilation via Error Subspace Statistical Estimation. Part II: Middle Atlantic Bight shelfbreak front simulations and ESSE validation, *Month. Weather Rev., 127*, 1408–1432, 1999a.

Lermusiaux, P.F.J., Estimation and study of mesoscale variability in the Strait of Sicily, *Dyn. Atm. Oceans, 29 (special issue)*, 255–303, 1999b.

Lermusiaux, P.F.J., and A.R. Robinson, Features of dominant mesoscale variability, circulation patterns and dynamics in the Strait of Sicily, *Deep-Sea Res. I, 48*, 1953–1997, 2001.

Lozano, C.J., P.J. Haley, Jr., H.G. Arango, Q. Sloan, and A.R. Robinson, Harvard coastal/deep water primitive equation model, *Harvard Open Ocean Model Reports, 52*, Harvard University, Cambridge, MA, 1994.

Lozano, C.J., A.R. Robinson, H.G. Arango, A. Gangopadhyay, Q. Sloan, P.J. Haley, Jr., L.A. Anderson, and W.G. Leslie, An interdisciplinary ocean prediction system: assimilation strategies and structured data models, in *Modern Approaches to Data Assimilation in Ocean Modeling*, edited by P. Malanotte-Rizzoli, *Elsevier Oceanography Series, 61*, Elsevier, 413–452, 1996.

Millot, C., Circulation in the Western Mediterranean Sea, *J. Mar. Syst., 20*, 424–442, 1999.

Onken, R., and J. Sellschopp, Water masses and circulation between the eastern Algerian Basin and the Strait of Sicily in October 1996. *Oceanol. Acta, 24*, 151–166, 2001.

Orlanski, I., A simple boundary condition for unbounded hyperbolic flows, *J. Comp. Phys., 21*, 251–269, 1976.

Pacanowski, R.C., and S.G.H. Philander, Parameterization of vertical mixing in numerical models of tropical oceans, *J. Phys. Oceanogr., 11*, 1443–1451, 1981.

Pierini, S., and A. Rubino, Modeling the oceanic circulation in the area of the Strait of Sicily: the remotely forced dynamics, *J. Phys. Oceanogr., 31*, 1397–1412, 2001.

Robinson, A.R., Physical processes, field estimation and an approach to interdisciplinary ocean modeling, *Earth-Science Rev., 40*, 3–54, 1996.

Robinson, A.R., Forecasting and simulating coastal ocean processes and variabilities with the Harvard Ocean Prediction System, in *Coastal Ocean Prediction*, edited by C.N.K. Mooers, *Coastal and Estuarine Studies Series*, American Geophysical Union, 77–100, 1999.

Robinson, A.R., H.G. Arango, A. Warn-Varnas, W.G. Leslie, A.J. Miller, P.J. Haley, Jr., and C.J. Lozano, Real-time regional forecasting, in *Modern Approaches to Data Assimilation in Ocean Modeling*, edited by P. Malanotte-Rizzoli, *Elsevier Oceanography Series, 61*, Elsevier, 377–410, 1996.

Robinson, A.R., and M. Golnaraghi, Circulation and dynamics of the Eastern Mediterranean Sea; quasi-synoptic data-driven simulations, *Deep-Sea Res. II, 40*, 1207–1246, 1993.

Robinson, A.R., P.F.J. Lermusiaux, and N.Q. Sloan, Data assimilation, in *The Sea, 10*, edited by K.H. Brink and A.R. Robinson, John Wiley & Sons, 541–594, 1998.

Robinson, A.R., J. Sellschopp, A. Warn-Varnas, W.G. Leslie, C.J. Lozano, P.J. Haley, Jr., L.A. Anderson, and P.F.J. Lermusiaux, The Atlantic-Ionian Stream, *J. Mar. Syst., 20*, 129–156, 2001.

Robinson, A.R., and L.J. Walstad, The Harvard open ocean model: Calibration and application to dynamical process forecasting and data assimilation studies, *J. Appl. Numer. Math., 3*, 89–121, 1987.

Sammari, C., C. Millot, I. Taupier-Letage, A. Stefani, and M. Brahmi, M., Hydrological characteristics in the Tunisia-Sardinia-Sicily area during spring 1995, *Deep-Sea Res. I, 46*, 1671–1703, 1999.

Shapiro, R., Smoothing, filtering, and boundary effects, *Rev. Geophys. Space Phys., 8*, 359–387, 1970.

Sloan, N.Q., Dynamics of a Shelf-Slope Front: Process Studies and Data-Driven Simulations in the Middle Atlantic Bight, Ph.D. Thesis, Harvard University, Cambridge,

MA, 230pp., 1996.

Spall, M.A., and A.R. Robinson, A new open ocean, hybrid coordinate primitive equation model, *Mathematics and Computers in Simulations, 31*, 241–269, 1989.

Spall, M.A., and A.R. Robinson, Regional primitive equation studies of the Gulf Stream meander and ring formation region, *J. Phys. Oceanogr. 20*, 985–1016, 1990.

Sparnocchia, S., G.P. Gasparini, M. Astraldi, M. Borghini, and P. Pistek, Dynamics and mixing of the Eastern Mediterranean outflow in the Tyrrhenian basin, *J. Mar. Syst. 20*, 301–317, 1999.

List of Figures

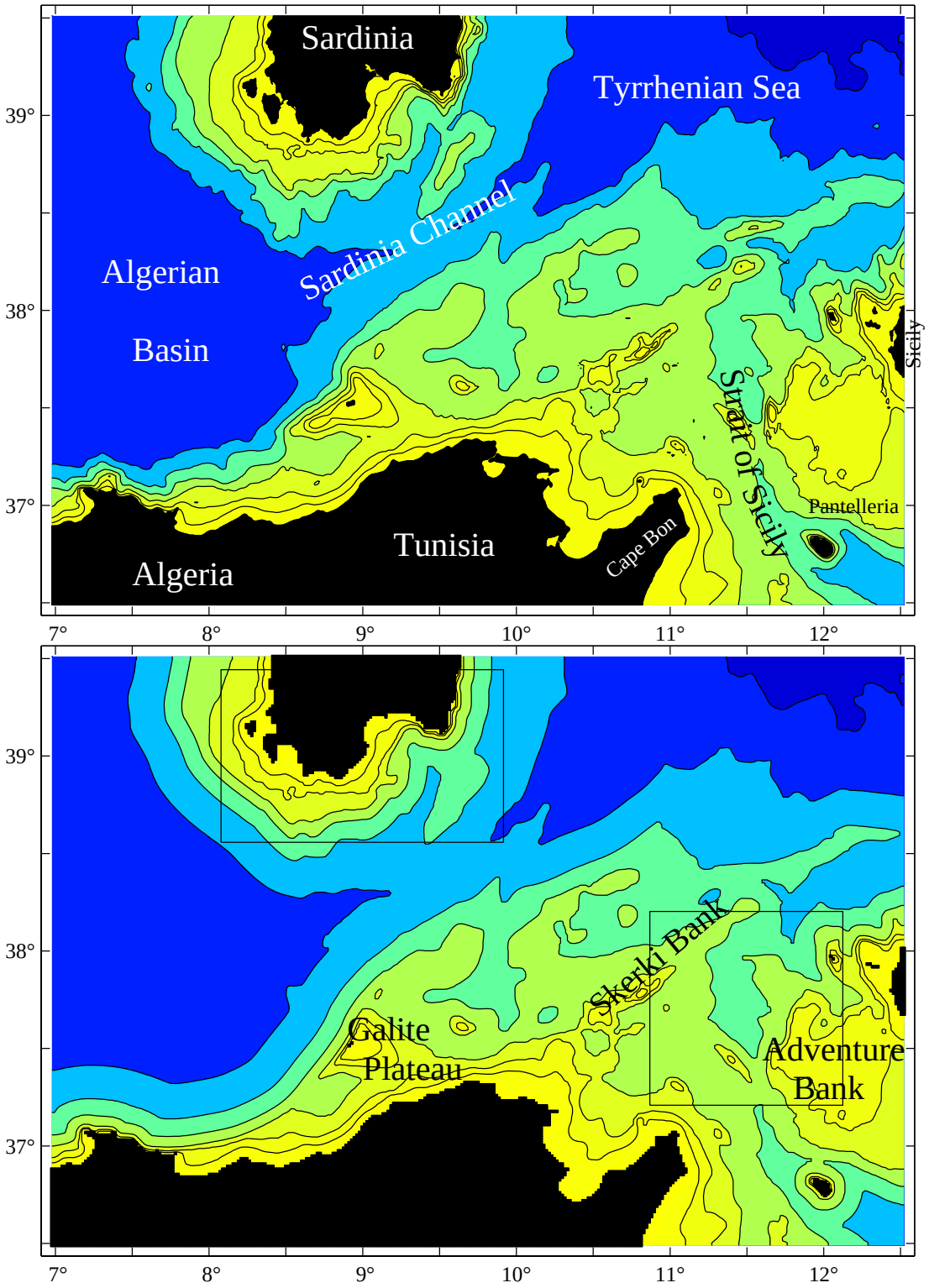

Figure 1: Original (top panel) and conditioned (bottom) model bathymetry of the large domain. Conditioning implies median filtering and reduction of bathymetric slopes to a maximum value of 6%. Note that most details of the bathymetry are preserved. Contour levels are drawn at 3000, 2000, 1000, 500, 200, 100, and 50-m water depth. The land areas (black) in the upper panel originate from a high-resolution coastline data set; in the lower panel, black areas are representing the land mask as it is used in the model. The rectangles indicate the position of the nested Sardinia and Sicily subdomain, respectively.

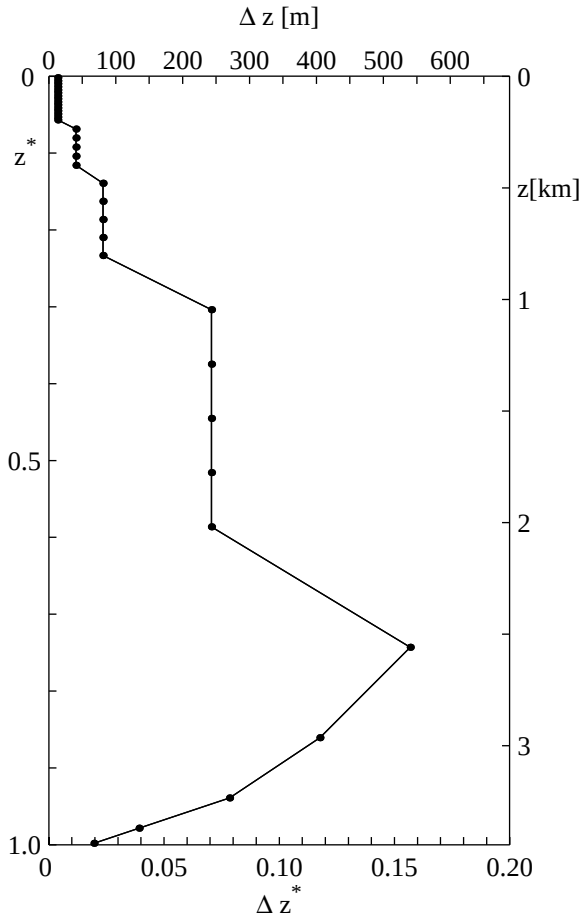

Figure 2: Thickness Δz of σ layers vs. depth z at the deepest model depth in the Tyrrhenian Sea (top and right axes). The bottom and and left axes show the non-dimensional layer thickness $\Delta z^* = \Delta z/H$ vs. non-dimensional depth $z^* = z/H$, where H is the water depth.

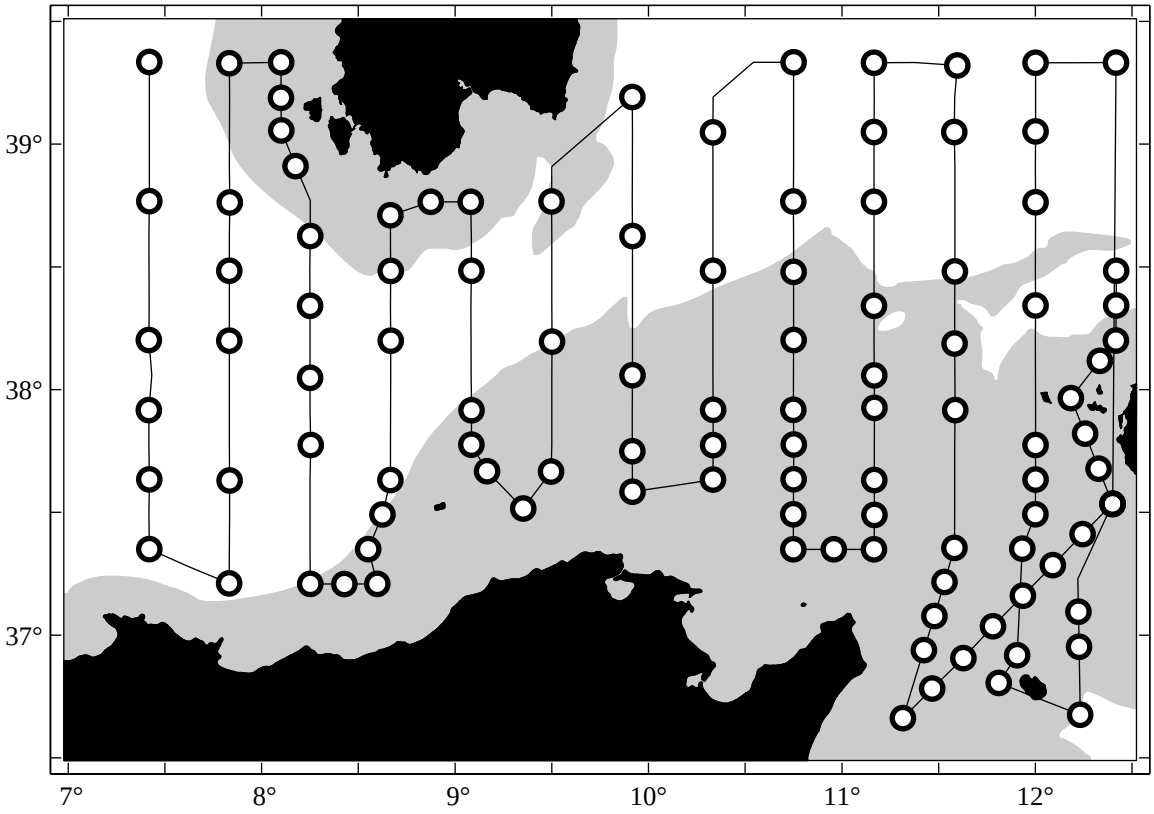

Figure 3: Ships's track (line) and positions of CTD and XCTD casts (circles) used for model initialization. The survey was accomplished from west to east. Water depths shallower than 1000 m are indicated by grey shading.

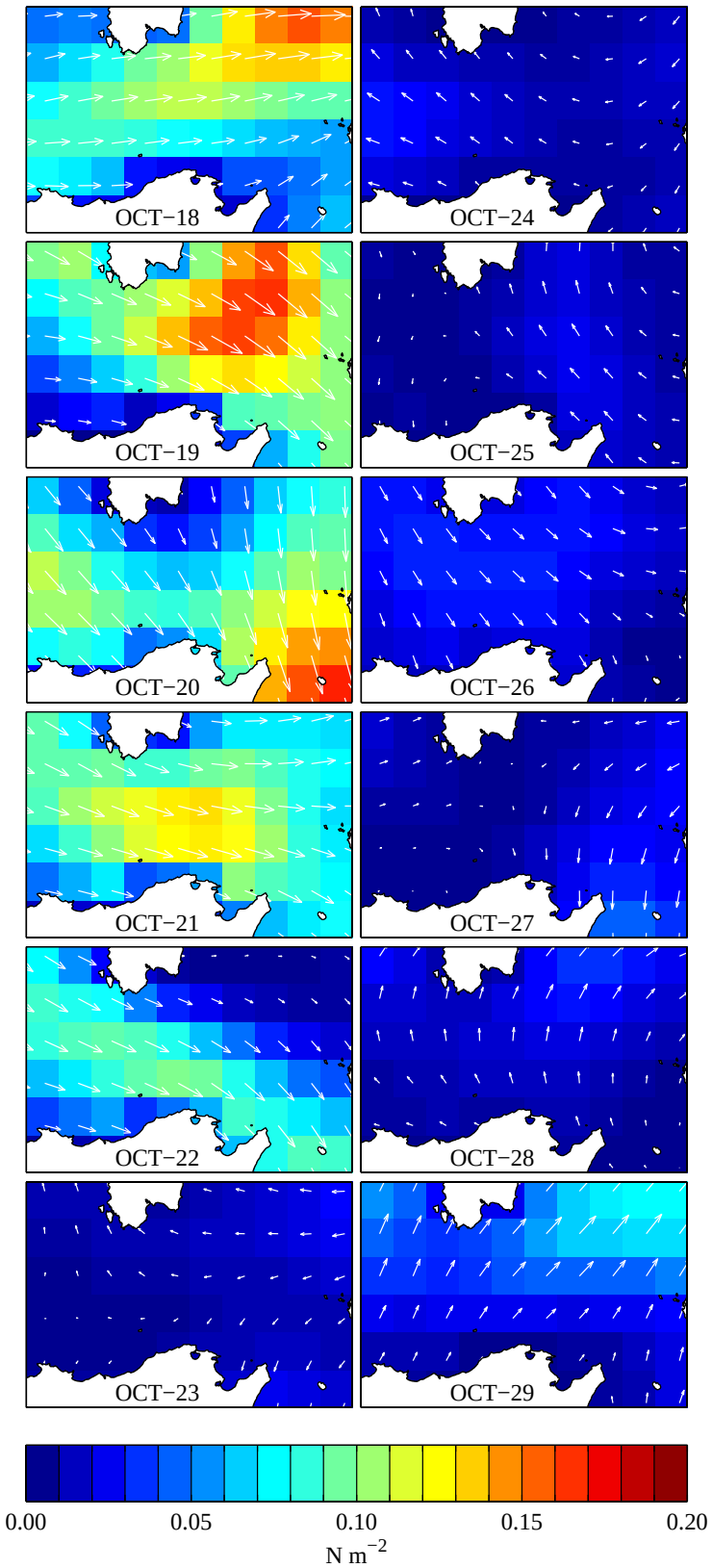

Figure 4: ECMWF noon windstress (color) and 10-m windspeed (vectors) 18–29 October. The maximum windspeed of close to 11 m s^{-1} is found on October 19 between Sardinia and Sicily.

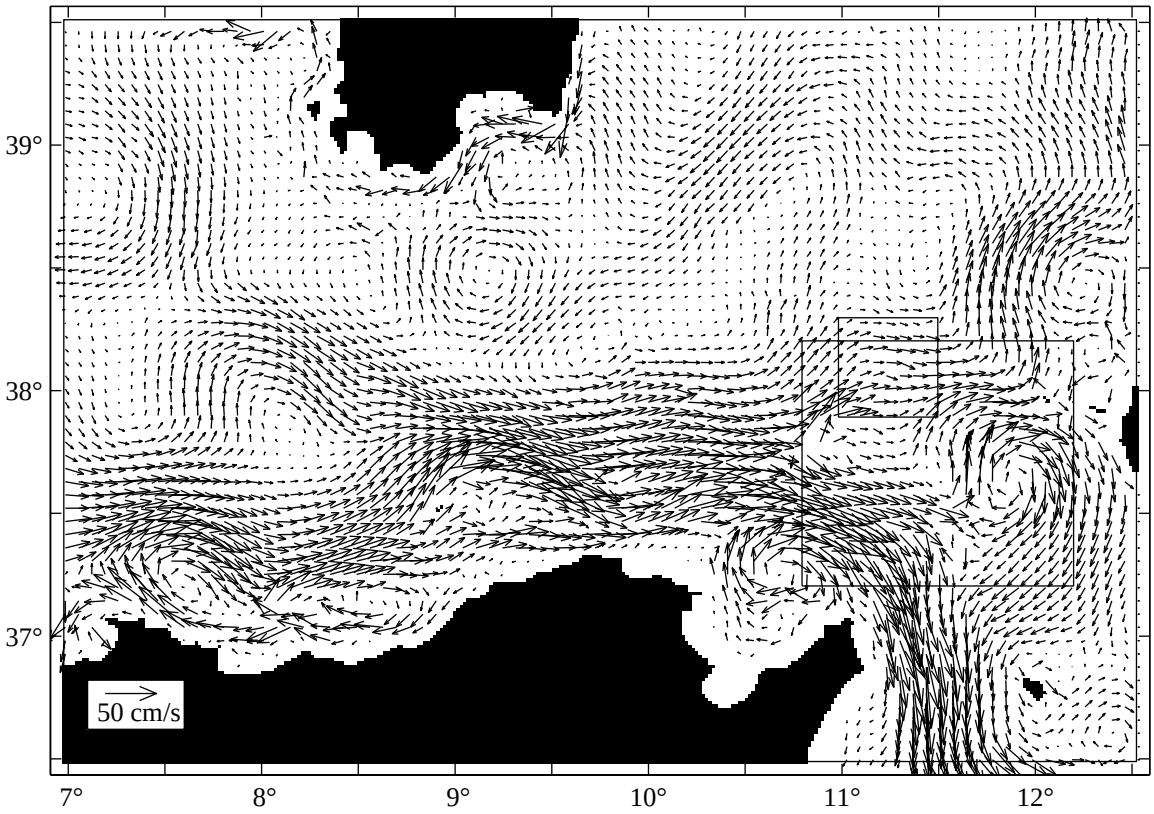

Figure 5: Time averaged flow of MAW at 30-m depth in the large domain (1500-m resolution, see Section 2.2). The vectors are plotted at 6-km resolution. The rectangles in the Strait of Sicily indicate the areas shown in Figs. 8 and 9, respectively. Areas where the water is shallower than 30 m are left white.

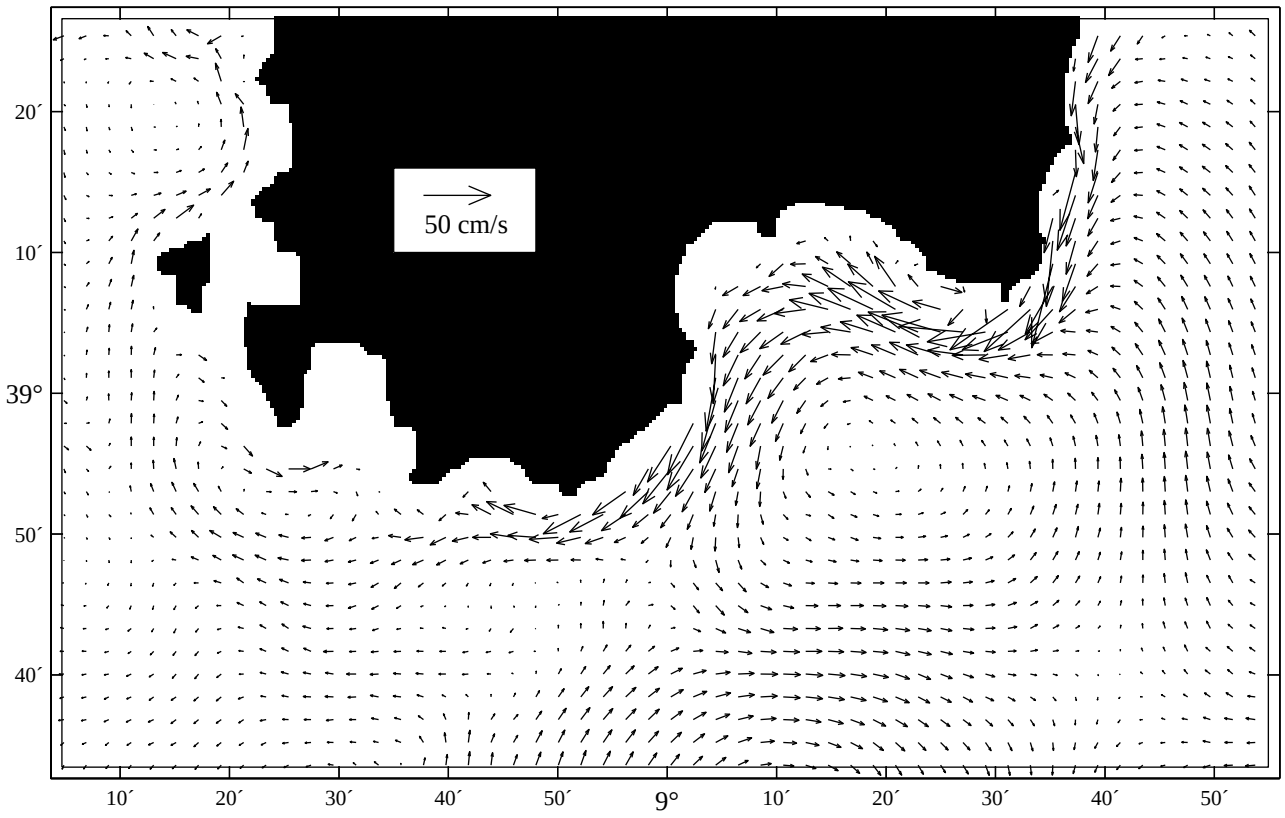

Figure 6: Time averaged flow of MAW at 30-m depth in the 2-way nested Sardinia subdomain (500-m resolution, see Sect. 2.2) . The resolution of the vectors plotted 3 km.

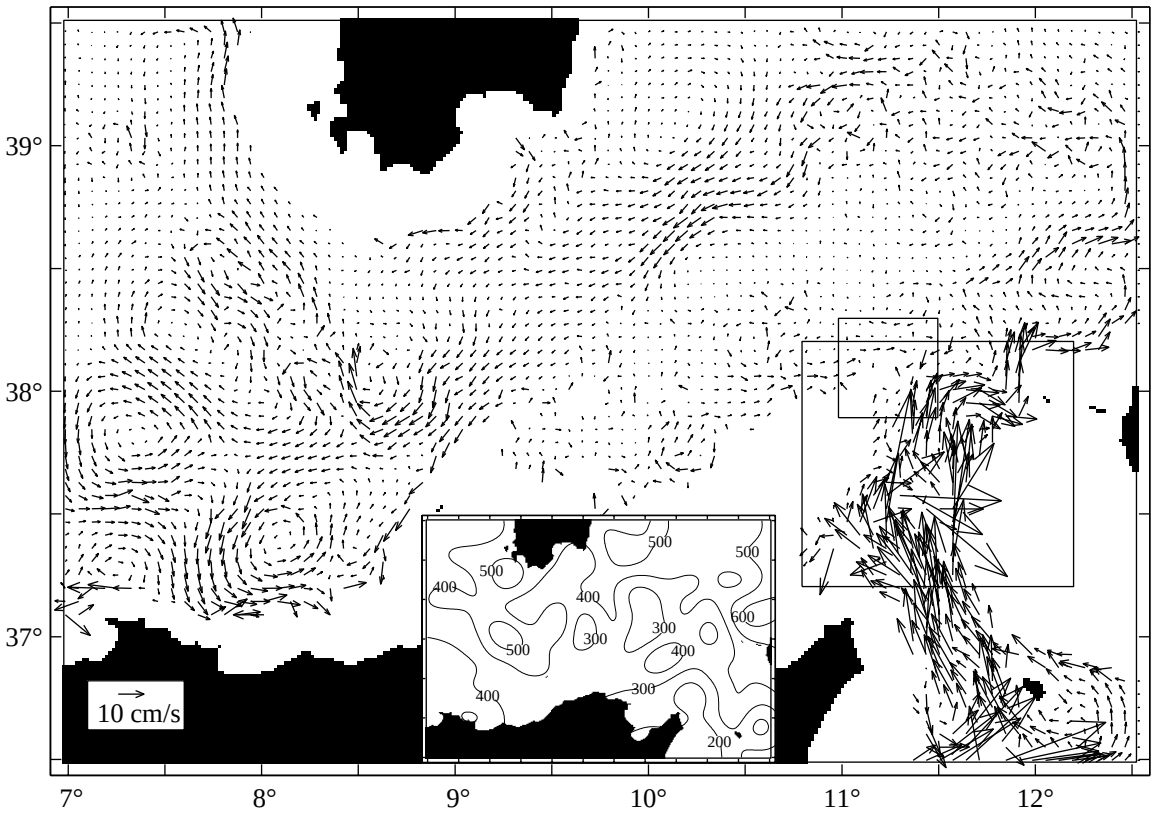

Figure 7: Time averaged LIW flow at the salinity maximum level in the large domain (1500-m resolution, see Sect. 2.2). The spacing between the vectors plotted is 6 km. The inset map shows the depth of the salinity maximum in dbar (from OS2001, Fig. 9). The rectangles in the northern Strait of Sicily indicate the areas shown in Fig. 8 and 9, respectively.

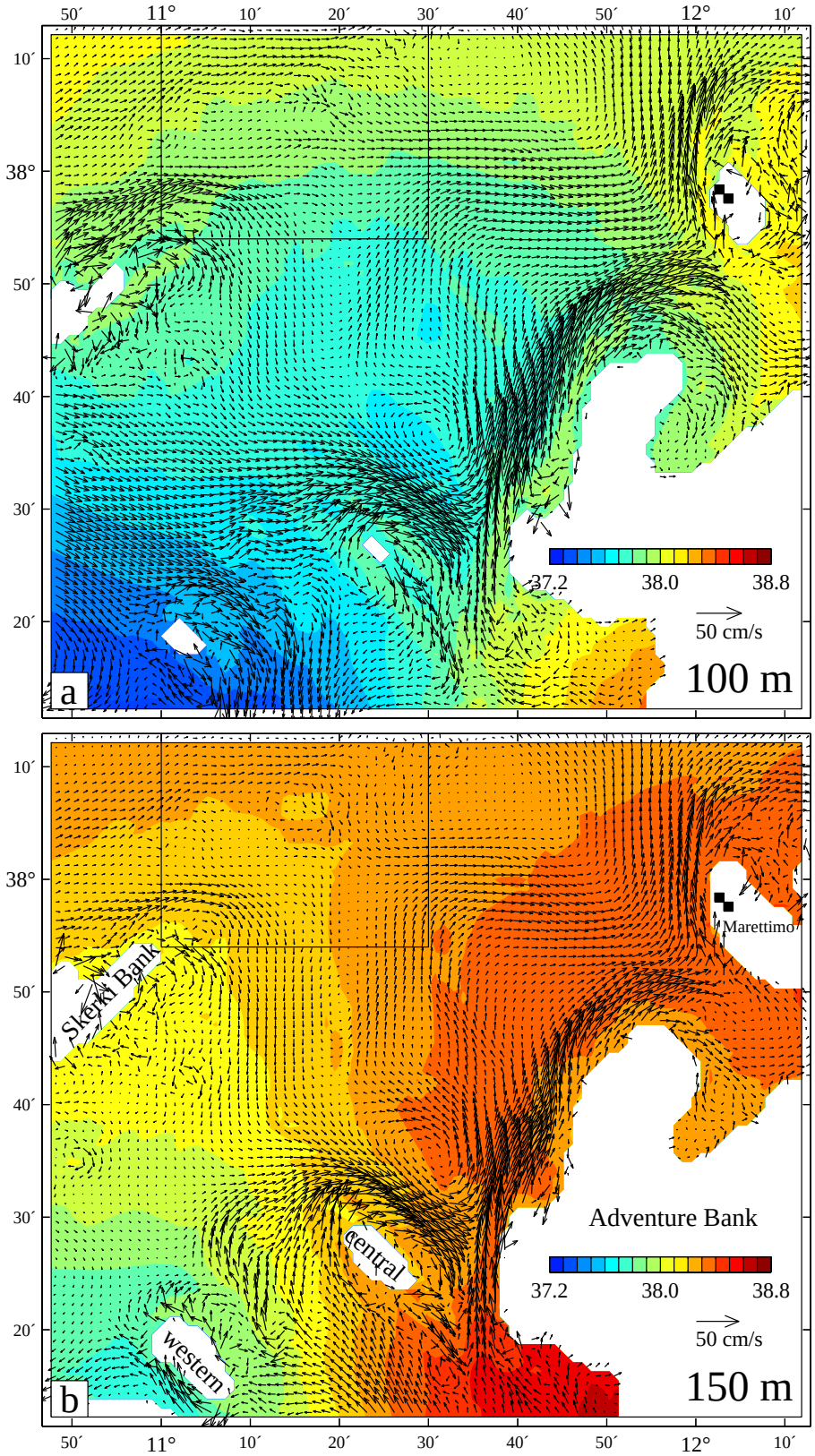

Figure 8: Time averaged salinity and currents west of the Adventure Bank at (a) 100 m, (b) 150 m, (c) 250 m, and (d) 400 m depth. Vectors are plotted at full resolution of 1.5 km. Areas where the water is shallower than the respective depth, are left white. The rectangle in the north refers to the area displayed in Fig. 9. Note the different velocity salinity scaling for (a),(b) and (c),(d), respectively.

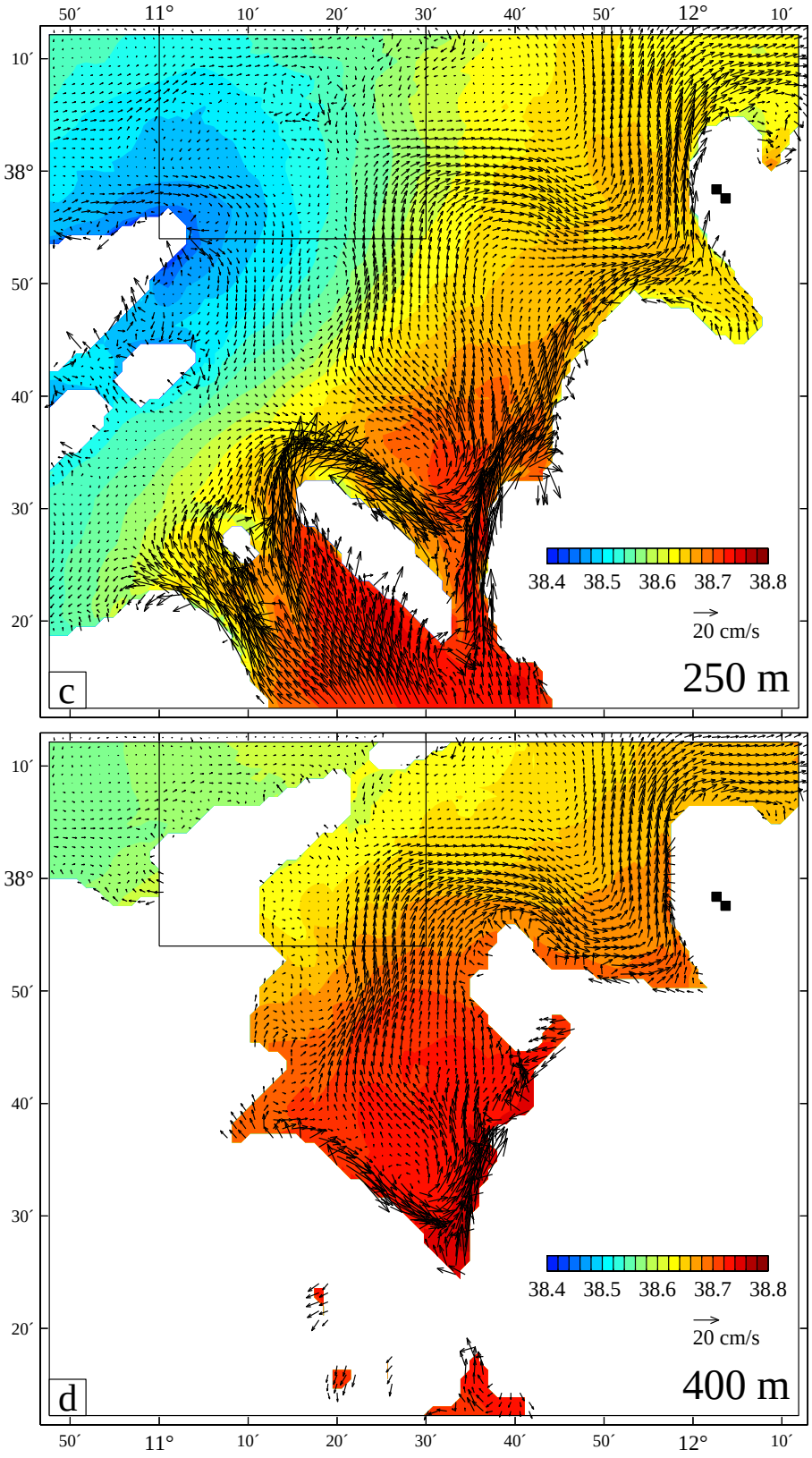

Figure 8: (continued)

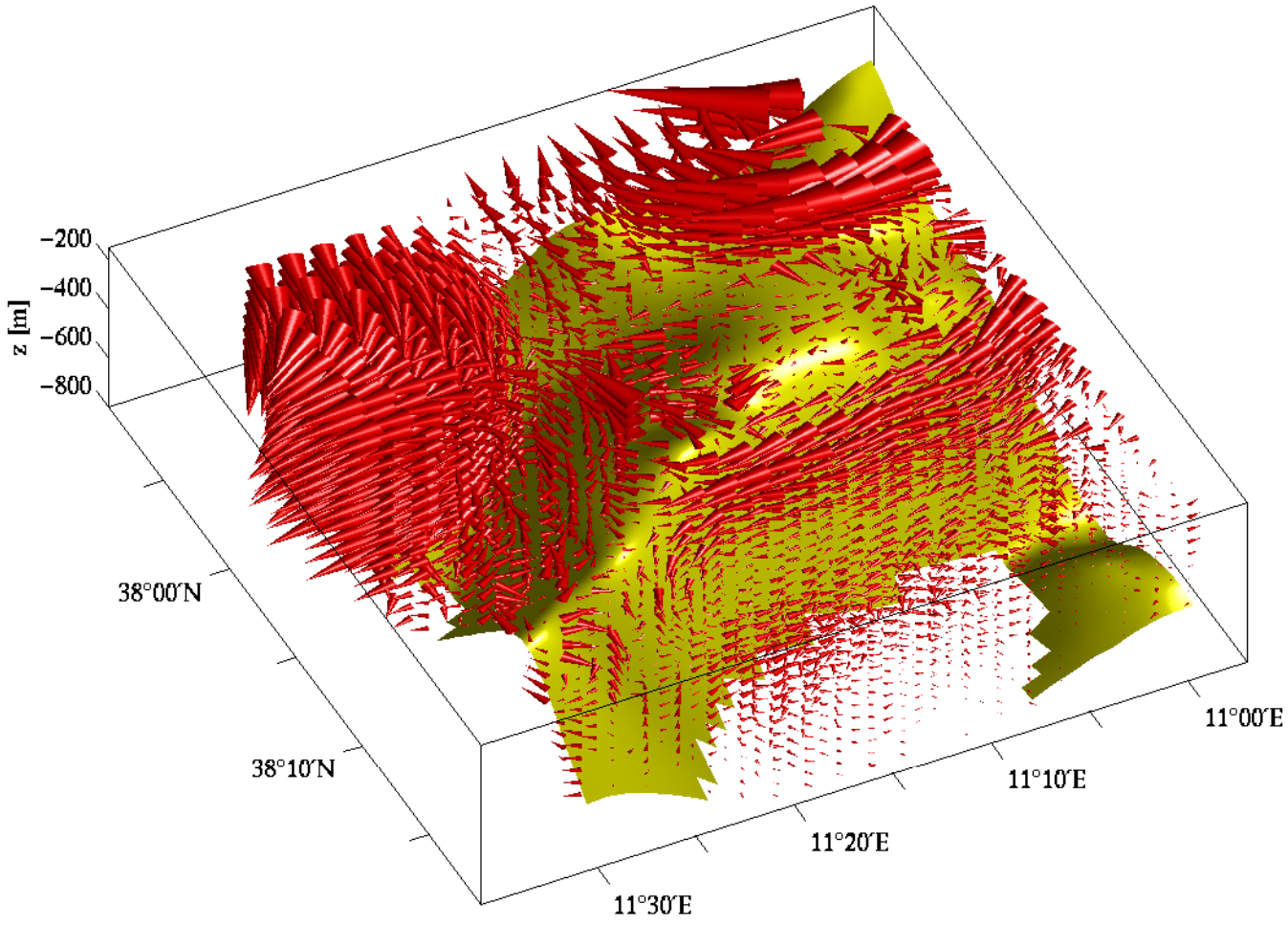

Figure 9: Three-dimensional view of the mean circulation around the northeastern extension of Skerki Bank in the 150 to 800-m depth range. The view direction is from northeast. The size of the cones is proportional to the speed; the maximum speed is 25 cm s^{-1} . Velocity components have been linearly interpolated on a horizontal grid spaced 1.5 times the model grid size, and vertically on constant depth levels in 50-m intervals. The model bathymetry is indicated by the yellow-shaded surface. For the position of the the cube, cf. Figs. 5, 7, and 8.

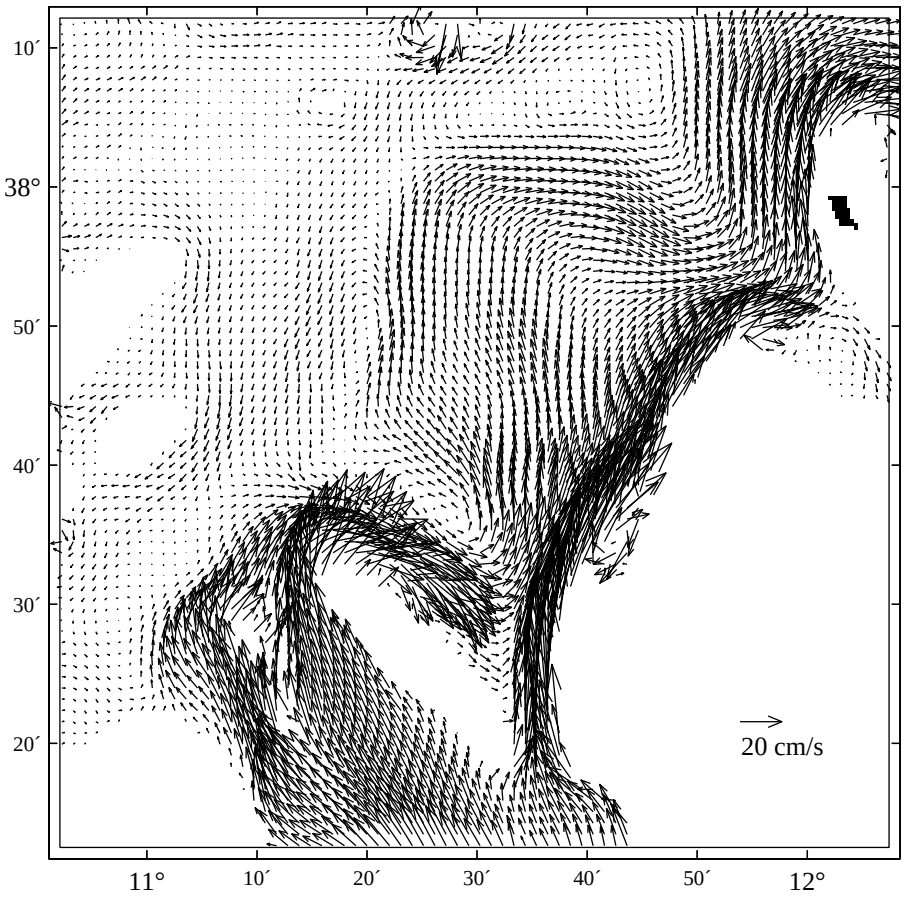

Figure 10: Time averaged currents at 250-m depth in the 2-way nested Sicily subdomain (500-m resolution, see Sect. 2.2). The vector spacing plotted is 1.5 km in order to match the horizontal resolution of Fig. 8c. Areas where the water is shallower than 250 m are left white.

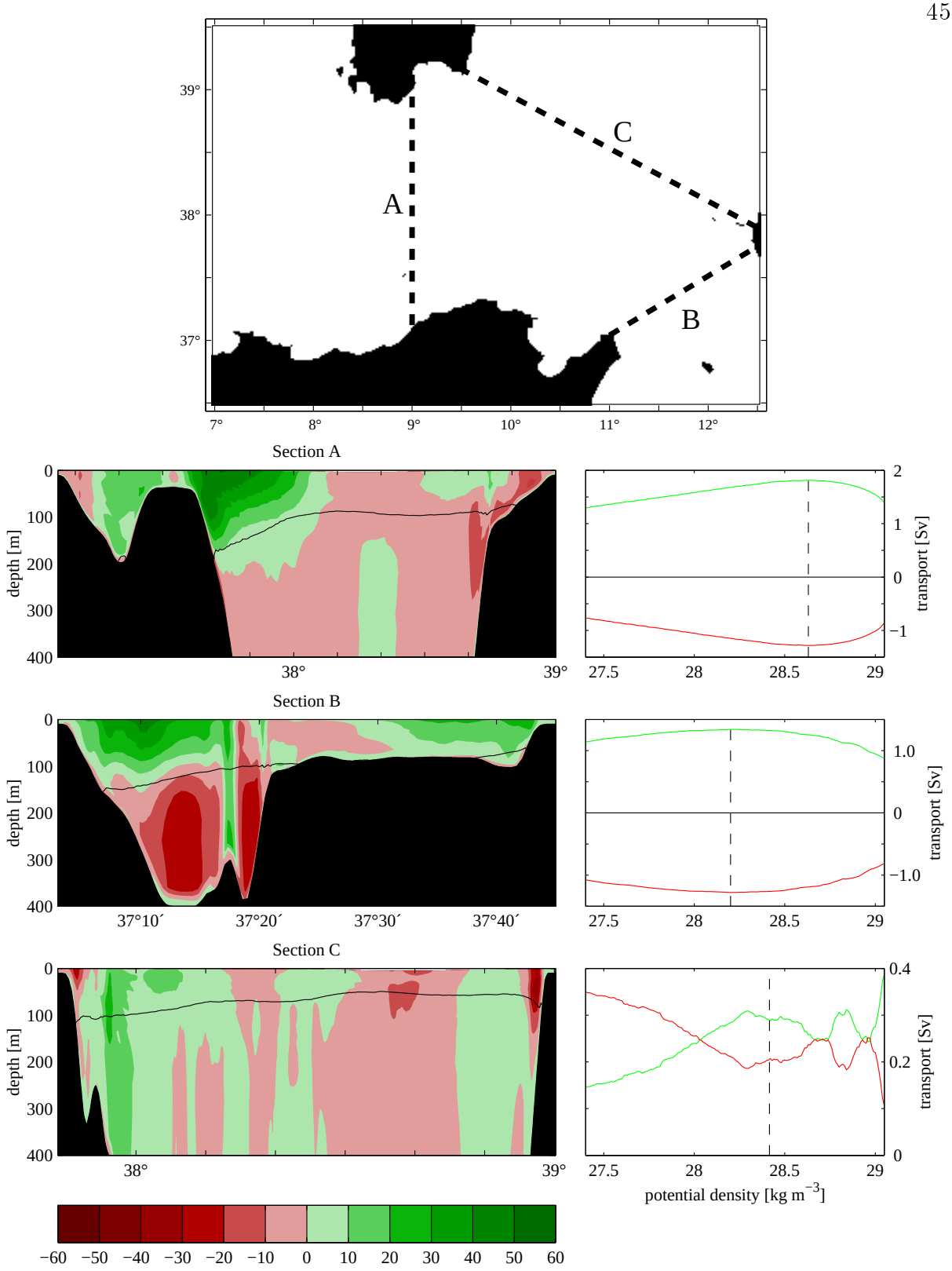

Figure 11: Normal mean velocity (left panel) and volume transport (right panel) across sections between Sardinia and Tunisia, Cape Bon and Sicily, and Sardinia and Sicily. In the velocity sections, green color code means eastward velocity in Section A, southeastward in B and northeastward in C. Opposite velocity components are indicated red. In the transport figures, MAW transport is indicated green, that of LIW red. Transport is plotted vs. potential density of the MAW/LIW interface. The dashed line refers to the isopycnal of the interface. In the velocity sections, the position of that isopycnal is indicated by the black line.

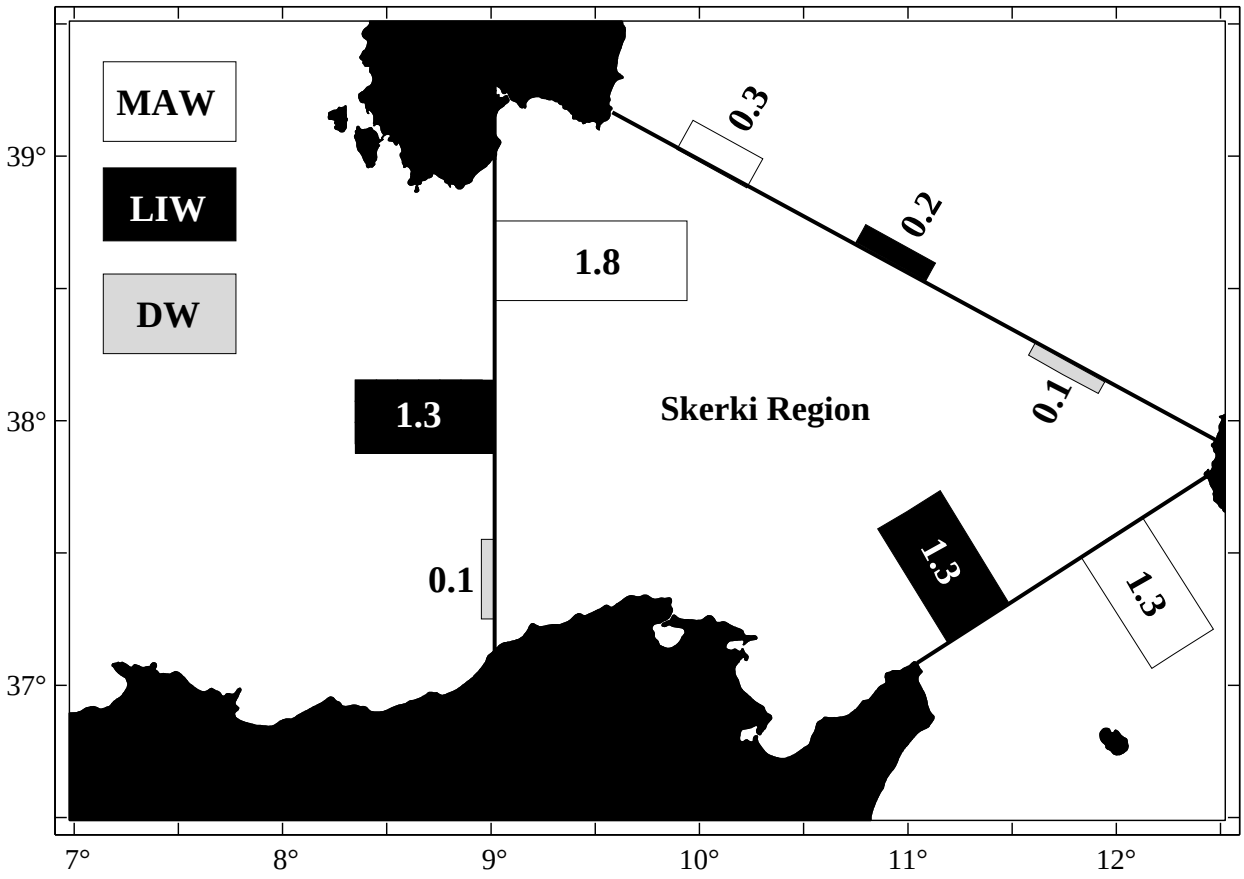

Figure 12: Net volume transports of MAW (white boxes), LIW (black) and DW (gray) between the Skerki region and neighboring basins across Sections A, B, and C (cf. Fig. 11). The length of the boxes is proportional to the transport, units are [Sv].